Int. J. Heat Mass Transfer. Vol. 36, No. 12, pp. 3069–3075, 1993
Printed in Great Britain

0017–9310/93 $6.00+0.00

Inverse segregation for a unidirectional solidification of aluminum–copper alloys

J. H. CHEN and H. L. TSAI

Department of Mechanical and Aerospace Engineering and Engineering Mechanics, University of Missouri—Rolla, Rolla, MO 65401, U.S.A.

(*Received* 11 *August* 1992 *and in final form* 14 *December* 1992)

Abstract—A mathematical model has been developed to simulate the inverse segregation for a unidirectional solidification of Al–Cu alloys cooled from the bottom. It is found from the present study that the fluid flow of solute-rich liquid in the mushy zone caused by solidification shrinkage is the main driving force for the formation of inverse segregation. The predicted copper concentration in the solidified alloys is in good agreement with the published experimental data. Several interesting transient behaviors of solute redistribution in the mushy zone, which were not reported before, are also discussed.

INTRODUCTION

FOR UNIDIRECTIONAL solidification of alloys cooled from the bottom, a higher concentration of solute exists in the solidified alloy near its bottom surface. This phenomenon, commonly called inverse segregation, was found experimentally as early as in 1540 [1]. It has been understood that the formation of inverse segregation for unidirectional solidification cooled from the bottom is caused by solidification contraction [2]. As for many alloys, the density of the solid phase is usually greater than that of the liquid phase; most alloys shrink 2–8% in volume during solidification. The shrinkage inevitably results in fluid flow in the solidifying alloy, causing the formation of inverse segregation.

Over the past decades, a variety of mathematical models have been proposed to simulate the formation of inverse segregation. Scheil [3] developed an expression which can predict only the 'maximum segregation' at the chill face as a function of alloy composition. Kirkaldy and Youdelis [4] extended the Scheil's equation to predict not only the maximum segregation, but also the positional variation of the segregation in a unidirectionally solidified ingot. But their model is limited to one-dimension, and the momentum, energy, and species equations are not completely coupled. Perhaps the first rigorous model to predict the formation of macrosegregation was described in the pioneering paper by Flemings and Nereo [1]. The well-known 'local solute redistribution equation' was derived which predicted successfully the formation of inverse segregation for unidirectional solidification of Al–Cu alloys [5]. The thermal gradients used in the local solute redistribution equation were measured based on seven thermocouples that were spaced evenly in the ingot along its centerline, and the velocity was obtained only by the simplified 'continuity equation'. Kato and Cahoon [6] studied the solute distribution in directionally solidified ingots containing an equiaxed structure and compared the experimental results with the theoretical calculations from the theory by Kirkaldy–Youdelis [4]. They showed that the experimental solute distribution agrees with the theoretical prediction, assuming the solid phase of equiaxed structure was stationary, for the first 50% of the ingot solidification. Ohnaka and Matsumoto [7] have analyzed the unidirectional solidification of Al–Cu alloys based on the conservation laws of mass, momentum, and energy using the direct finite difference method [8]. They compared their simulated solute distribution in the solidified alloy with the measured and calculated results by Kato and Cahoon [6], but they did not show the transient fluid flow patterns and solute distributions in the alloy.

The volumetric averaging formulation recently proposed by Beckermann and Viskanta [9] allows the calculations of multi-dimensional fluid flow and heat and mass transfer in the solidifying alloy. Using this formulation, while it has been possible to qualitatively predict some of the phase-change and double-diffusive phenomena observed in the experiments, the numerical simulation shows considerable disagreement with the measurements [9]. Neilson and Incropera [10] studied the unidirectional solidification of aqueous NH_4Cl and the effects of the compositionally induced fluid motion. Because aqueous NH_4Cl liquid within the mushy region is enriched by the lighter H_2O species as solid NH_4Cl is precipitated, a density inversion is created leading to an unstable large-scale channel-like, double-diffusive natural convection, which gives rise to pronounced freckle formation [10]. Their solidification model employed mathematical formulations based on the assumption that shrinkage-induced fluid flow was negligible.

For the solidification of Al–Cu alloys, because the

NOMENCLATURE

c	specific heat
C	inertial coefficient
c_1	permeability coefficient
d	dendrite arm spacing
D	mass diffusion coefficient
f	mass fraction
g	volume fraction or gravitational acceleration
h	enthalpy
H	cavity height or latent heat of solidification
h_c	heat transfer coefficient between casting and chill
K	permeability
k_p	equilibrium partition ratio (m_{liq}/m_{sol})
k	thermal conductivity
m	slope
p	pressure
T	temperature
T_c	chill temperature
T_m	fusion temperature as $f^\alpha \to 0$
t	time
u	flow velocity in x direction
$\mathbf{V}$	velocity vector
$\mathbf{V}_r$	relative velocity vector between liquid phase and solid phase ($\mathbf{V}_l - \mathbf{V}_s$)
v	flow velocity in y direction
W	cavity width
x	x coordinate
y	y coordinate.

Greek symbols

β_s	solutal expansion coefficient
β_T	thermal expansion coefficient
μ	dynamic viscosity
ρ	density.

Subscripts

e	eutectic
k	phase k
l	liquid phase
liq	liquidus
o	initial
s	solid phase
sol	solidus.

Superscript

α	constituent α.

mushy region adjacent to the bottom chill is enriched by the heavier copper species, as solid aluminum is precipitated, it presents stable vertical temperature and solute gradients. In other words, no fluid flow can be created if the shrinkage effect is neglected. In fact, shrinkage-induced flow will be the only driving force to form the inverse segregation for a unidirectional solidification of Al–Cu alloys cooled from the bottom. Hence, the inverse segregation in Al–Cu alloys cannot be predicted if the shrinkage-induced flow is neglected. The continuum equations developed by Bennon and Incropera [11] have been modified by Chiang and Tsai [12, 13] to include the shrinkage-induced flow. In this study, the continuum model including the shrinkage-induced fluid flow will be utilized to predict the inverse segregation for a unidirectional solidification of Al–Cu alloys.

MATHEMATICAL FORMULATION

For two-dimensional solidification of alloys, the governing differential equations based on the continuum formulation including shrinkage-induced effect and thermosolutal convection derived previously [12–14] will be used in the present study. The continuity, momentum, energy, and species equations can be expressed as

Continuity

$$\frac{\partial}{\partial t}(\rho)+\nabla\cdot(\rho\mathbf{V})=0 \tag{1}$$

Momentum

$$\frac{\partial}{\partial t}(\rho u)+\nabla\cdot(\rho\mathbf{V}u)=\nabla\cdot\left(\mu_l\frac{\rho}{\rho_l}\nabla u\right)-\frac{\partial p}{\partial x}$$
$$-\frac{\mu_l}{K}\frac{\rho}{\rho_l}(u-u_s)-\frac{C\rho^2}{K^{1/2}\rho_l}|u-u_s|(u-u_s)$$
$$-\nabla\cdot(\rho f_s f_l\mathbf{V}_r u_r)+\nabla\cdot\left(\mu_l u\nabla\left(\frac{\rho}{\rho_l}\right)\right) \tag{2}$$

$$\frac{\partial}{\partial t}(\rho v)+\nabla\cdot(\rho\mathbf{V}v)=\nabla\cdot\left(\mu_l\frac{\rho}{\rho_l}\nabla v\right)-\frac{\partial p}{\partial y}$$
$$-\frac{\mu_l}{K}\frac{\rho}{\rho_l}(v-v_s)-\frac{C\rho^2}{K^{1/2}\rho_l}|v-v_s|(v-v_s)$$
$$-\nabla\cdot(\rho f_s f_l\mathbf{V}_r v_r)+\nabla\cdot\left(\mu_l v\nabla\left(\frac{\rho}{\rho_l}\right)\right)$$
$$+\rho g(\beta_T(T-T_o)+\beta_s(f_l^\alpha-f_{l,o}^\alpha)) \tag{3}$$

Energy

$$\frac{\partial}{\partial t}(\rho h)+\nabla\cdot(\rho\mathbf{V}h)=\nabla\cdot\left(\frac{k}{c_s}\nabla h\right)$$
$$+\nabla\cdot\left(\frac{k}{c_s}\nabla(h_s-h)\right)-\nabla\cdot(\rho(\mathbf{V}-\mathbf{V}_s)(h_l-h)) \tag{4}$$

Species

$$\frac{\partial}{\partial t}(\rho f^{\alpha})+\nabla\cdot(\rho\mathbf{V}f^{\alpha})=\nabla\cdot(\rho D\nabla f^{\alpha})$$
$$+\nabla\cdot(\rho D\nabla(f_{\mathrm{l}}^{\alpha}-f^{\alpha}))-\nabla\cdot(\rho(\mathbf{V}-\mathbf{V}_{\mathrm{s}})(f_{\mathrm{l}}^{\alpha}-f^{\alpha})). \tag{5}$$

In the above equations, the continuum density, specific heat, thermal conductivity, mass diffusivity, solid mass fraction, liquid mass fraction, velocity, enthalpy, and mass fraction of constitute α are defined as follows:

$$\rho=g_{\mathrm{s}}\rho_{\mathrm{s}}+g_{\mathrm{l}}\rho_{\mathrm{l}},\quad c=f_{\mathrm{s}}c_{\mathrm{s}}+f_{\mathrm{l}}c_{\mathrm{l}},\quad k=g_{\mathrm{s}}k_{\mathrm{s}}+g_{\mathrm{l}}k_{\mathrm{l}}$$
$$D=f_{\mathrm{s}}D_{\mathrm{s}}+f_{\mathrm{l}}D_{\mathrm{l}};\quad f_{\mathrm{s}}=\frac{g_{\mathrm{s}}\rho_{\mathrm{s}}}{\rho};\quad f_{\mathrm{l}}=\frac{g_{\mathrm{l}}\rho_{\mathrm{l}}}{\rho}$$
$$\mathbf{V}=f_{\mathrm{s}}\mathbf{V}_{\mathrm{s}}+f_{\mathrm{l}}\mathbf{V}_{\mathrm{l}};\quad h=f_{\mathrm{s}}h_{\mathrm{s}}+f_{\mathrm{l}}h_{\mathrm{l}};\quad f^{\alpha}=f_{\mathrm{s}}f_{\mathrm{s}}^{\alpha}+f_{\mathrm{l}}f_{\mathrm{l}}^{\alpha}. \tag{6}$$

In the above governing differential equations (1)–(5), there is a solid phase velocity. Under the condition of unidirectional solidification cooled from the bottom, to be considered in the present study, the solid phase is likely to be stationary. Hence, we assume the solid phase velocity is zero ($\mathbf{V}_{\mathrm{s}}=0$), and the equations are simplified accordingly.

The phase enthalpy is defined as

$$h_{\mathrm{k}}=\int_0^T c_{\mathrm{k}}\,\mathrm{d}T. \tag{7}$$

If the phase specific heats are further assumed constant, phase enthalpies by equation (7) are expressed as

$$h_{\mathrm{s}}=c_{\mathrm{s}}T;\quad h_{\mathrm{l}}=c_{\mathrm{l}}T+(c_{\mathrm{s}}-c_{\mathrm{l}})T_{\mathrm{e}}+H. \tag{8}$$

The assumption of permeability in the mushy region requires consideration of the growth morphology specific to the system under consideration. In analogy to flow in porous media, the permeability K is calculated using the Carman–Kozeny equation [15]

$$K=\frac{g_{\mathrm{l}}^3}{c_{\mathrm{l}}(1-g_{\mathrm{l}})^2} \tag{9}$$

where the value of c_{l} depends on the morphology of the porous media. In the present study c_{l} can be expressed as [16]

$$c_{\mathrm{l}}=\frac{180}{d^2} \tag{10}$$

where d is assumed to be a constant and is of the order of 10^{-2} cm. Similarly, the inertial coefficient, C, can be calculated from [17]

$$C=0.13g_{\mathrm{l}}^{-3/2}. \tag{11}$$

In the pure solid phase ($g_{\mathrm{l}}=0$) and pure liquid phase ($g_{\mathrm{l}}=1$), equation (9) reduces to the appropriate limits, namely, $K=0$ and $K=\infty$, respectively.

Closure of the system of conservation equations requires supplementary relationships for the phase mass fraction f_{k} and composition f_{k}^{α}. With the assumption of local equilibrium, the required expressions may be obtained from the equilibrium phase diagram. Neglecting solidus and liquidus line curvature, the solid mass fraction and phase compositions can be expressed as [2]

$$f_{\mathrm{s}}=\frac{1}{1-k_{\mathrm{p}}}\left[\frac{T-T_{\mathrm{liq}}}{T-T_{\mathrm{m}}}\right];\quad f_{\mathrm{s}}^{\alpha}=\left[\frac{k_{\mathrm{p}}}{1+f_{\mathrm{s}}(k_{\mathrm{p}}-1)}\right]f^{\alpha};$$
$$f_{\mathrm{l}}^{\alpha}=\left[\frac{1}{1+f_{\mathrm{s}}(k_{\mathrm{p}}-1)}\right]f^{\alpha} \tag{12}$$

where T_{liq} is the liquidus temperature corresponding to f^{α}, T_{m} is the fusion temperature as $f^{\alpha}\to 0$, and the equilibrium partition ratio k_{p} is the ratio of the slopes for liquidus and solidus lines ($k_{\mathrm{p}}=m_{\mathrm{liq}}/m_{\mathrm{sol}}$).

The study was performed for a rectangular geometry of width W and height H. The rectangular cavity contains an Al–Cu alloy liquid, initially at uniform temperature and uniform copper species concentration. Unidirectional solidification was induced by placing a chill at the bottom with a finite heat transfer coefficient h_{c} and constant chill temperature T_{c}. Adiabatic boundary conditions were imposed on the other walls. As the velocity of shrinkage-induced fluid flow, in general, is small, the free surface is considered to be flat. Hence, the effect of surface tension can be neglected. The boundary conditions on the free surface at the top of the domain are free of normal and tangential stress. In summary, the boundary conditions for governing equations (1)–(5) can be written as

(1)

$$\text{at}\quad x=0:u=0,\quad \frac{\partial v}{\partial x}=0,\quad \frac{\partial T}{\partial x}=0,\quad \frac{\partial f^{\alpha}}{\partial x}=0 \tag{13a}$$

(2)

$$\text{at}\quad x=\frac{W}{2}:u=0,\quad v=0,\quad \frac{\partial T}{\partial x}=0,\quad \frac{\partial f^{\alpha}}{\partial x}=0 \tag{13b}$$

(3)

$$\text{at}\ y=0:u=0,\quad v=0,$$
$$-k\frac{\partial T}{\partial y}=h_{\mathrm{c}}(T-T_{\mathrm{c}}),\quad \frac{\partial f^{\alpha}}{\partial y}=0 \tag{13c}$$

(4)

$$\text{at}\quad y=H:p=0,\quad \frac{\partial u}{\partial y}=0,\quad \frac{\partial T}{\partial y}=0,\quad \frac{\partial f^{\alpha}}{\partial y}=0 \tag{13d}$$

where p is the gage pressure.

The above coupled continuity, momentum, energy, and species equations, subjected to the required boun-

Table 1. Thermophysical properties for Al–4.1% Cu alloys, casting conditions, and geometric data

Symbol	Value	Reference
c_s	1.0928 J g^{-1} K^{-1}	[18]
c_l	1.0588 J g^{-1} K^{-1}	[18]
D_l^z	3×10^{-5} cm^2 s^{-1}	($D_l^z \gg D_s^z \cong 0$) assumed
k_s	1.9249 W cm^{-1} K^{-1}	[18]
k_l	0.8261 W cm^{-1} K^{-1}	[18]
k_p	0.170	[18]
m_{liq}	−337.35 K (wt frac.)$^{-1}$	[18]
ρ_s	2.65 g cm^{-3}	[18]
ρ_l	2.40 g cm^{-3}	[18]
β_T	4.95×10^{-5} K^{-1}	assumed
β_s	−2.0	assumed
μ	0.03 g cm^{-1} s^{-1}	[18]
H	397.5 J g^{-1}	[18]
T_e	821.2 K	[18]
T_m	933.2 K	[18]
f_{Lo}^z	4.1%	
T_o	970.0 K	
T_c	293.0 K	
h_c	0.0837 W cm^{-2} K^{-1}	
H	15.0 cm	
W	4.0 cm	

dary conditions, were solved by an implicit control-volume-based finite difference procedure using the SIMPLEC algorithm. The domain change due to solidification shrinkage was handled by the front tracking method. Detailed discussions about the numerical method and the check of numerical accuracy were given in the previous papers [12, 13], and will not be repeated here. All the calculations were executed on Apollo DN10 000 workstations, and typical CPU time for the calculation of each case is about 100 h.

RESULTS AND DISCUSSION

The thermophysical properties for Al–4.1% Cu alloys, casting conditions, and geometric data are given in Table 1. The mushy region and fluid flow field at the selected grid points are shown in Fig. 1 at times t = 16.0, 186.0, and 296.0 s, respectively. The solidus and liquidus interfaces shown in the figure indicate the boundaries between the solid region, the mushy region, and the liquid region. The horizontal solidus and liquidus interfaces implies that the isotherms are planar, which is expected for the unidirectional solidification. Due to a fine permeable matrix (dendrites) within the mushy zone, the velocities in this region are smaller than those in the liquid region. Even though the velocity is small within the mushy region, such a fluid flow could be significant in determining the formation of inverse segregation. As an isotropic permeability of the mushy region is incorporated into the model, the fluid flow through the liquidus interface and into the mushy region, shown in Fig. 1, is similar to the phenomena of water being absorbed by a spongy material. The velocity profile in the mushy zone is uniform at each horizontal cross-section. One can see that a W-shaped velocity profile in the liquid region gradually extends to the top of the domain from the liquidus interface as time increases. In Fig. 1(c), the velocities are zero in the solid region.

As the casting is cooled from the bottom, a stable thermal field should be developed in the casting. Hence, the W-shaped velocity profile can only be possibly caused by the composition gradients and/or shrinkage effect in the casting. In order to study this, calculations were performed when natural convection due to temperature and composition gradients was neglected and only the shrinkage effect was included. Under this condition, the transient development of the solidus and liquidus contours and velocity plots at selected grids, which may be compared with that of Fig. 1, are shown in Fig. 2. The obvious difference between Fig. 1 and Fig. 2 is the velocity field within the bulk liquid region. A parabolic-shape of velocity profiles is obtained if only the shrinkage effect is considered. The velocity profiles of both figures, across the horizontal section of a distance 12.5 cm from the bottom chill, at time t = 296.0 s is shown in Fig. 3. The flow rates integrated using the trapezoidal rule are 9.3883714×10^{-3} cm^2 s^{-1} and 9.3886172×10^{-3} cm^2 s^{-1} for Figs. 2 and 3, respectively. These two values are almost the same to maintain the overall mass conservation. The actual mechanism to cause a W-shaped velocity will be discussed later. It is found that the isotherms in both Figs. 2 and 3 are planar, and they are not influenced by the shape of the velocity profiles in the liquid phase. Also, the flow patterns in the mushy region and the copper species distributions, to be discussed next, are nearly identical whether the natural convection due to temperature and composition gradients is included or not. This implies that the shrinkage-induced flow is the main driving force for the solute redistribution in the mushy region leading to the formation of inverse segregation.

The contours of constant species concentration corresponding to the various times in Fig. 1 are shown in Fig. 4. The isocompositions are also planar, as the isotherms, and are spaced 0.01% apart in Fig. 4(a) and 0.05% apart in Figs. 4(b) and (c). It is seen that the spacing between isocompositions does not decrease or increase monotonically upward as the temperature field does, and there is a minimum copper concentration in the middle of the casting. Figure 5 shows the species concentration distributions along the centerline at various times. It is seen that a solute-rich (i.e. copper concentration is higher than the initial value) region is obtained in the vicinity of the chill, and then followed by a solute-depleted (i.e. copper concentration is lower than the initial value) region to ensure the conservation of total solute. It should be noted that the change of copper concentration is created due to the rejection of copper species in the mushy zone during solidification. The positive segregation near the chilled wall is caused by the flow of solute-rich liquid against the chill, leading to the pile up of solute near the bottom of the casting. Hence,

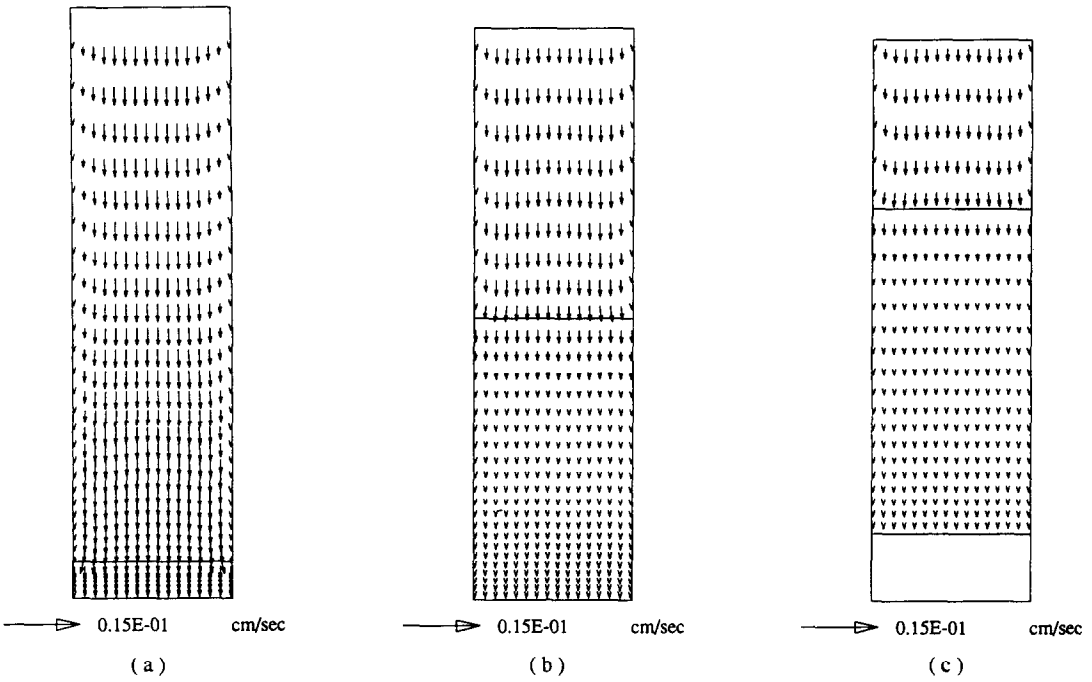

FIG. 1. The predicted flow patterns and mushy zones at times: (a) $t = 16.0$ s; (b) $t = 186.0$ s; (c) $t = 296.0$ s.

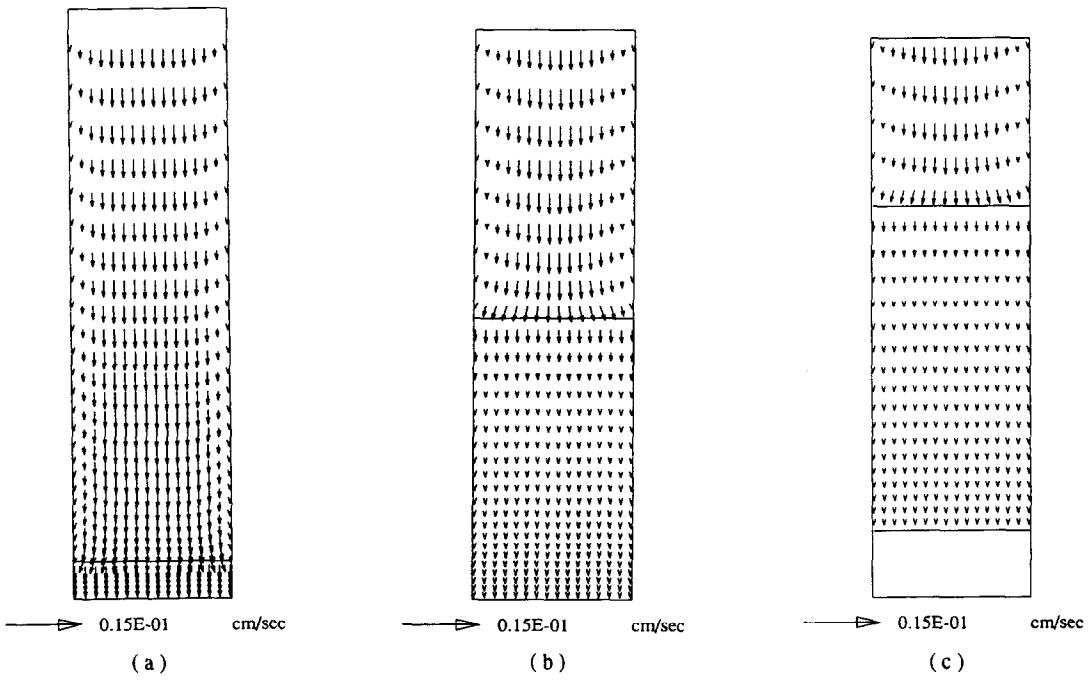

FIG. 2. The predicted flow patterns and mushy zones for shrinkage effect only at times: (a) $t = 16.0$ s; (b) $t = 186.0$ s; (c) $t = 296.0$ s.

the formation of inverse segregation is understood to be caused by the shrinkage-induced flow within the mushy zone. It is also seen that the slopes of curves 3 and 4 change suddenly near the solidus interface, and these two curves merge together within the completely solidified region, because the transport of copper species in the solid region is negligible. The concentration remains at the initial value in the liquid region.

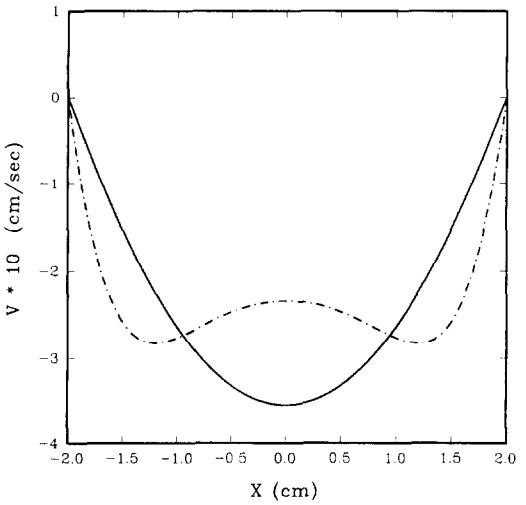

FIG. 3. A comparison of velocity profiles, across the horizontal cross section of a distance 12.5 cm from the bottom chill, between Figs. 1 and 2 at time $t = 296.0$ s.

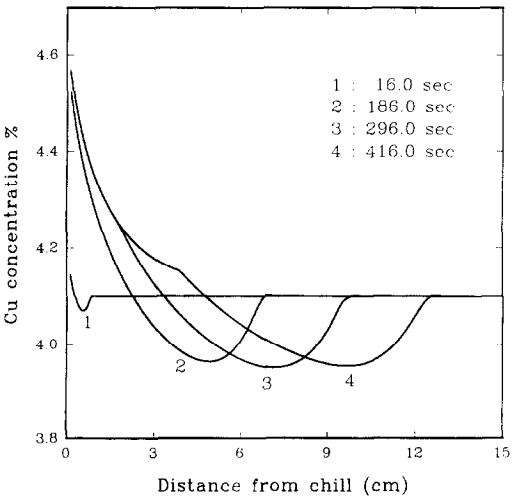

FIG. 5. The predicted solute distributions along the centerline at times $t = 16.0$, 186.0, 296.0, 416.0 s.

As revealed by Fig. 5, positive solutal gradients exist near the liquidus interface, so a buoyancy force induced by the density inversion is transported into the bulk liquid region from the liquidus interface. Such a condition leads to the W-shaped velocity profile shown in Fig. 1. It is interesting to notice that the W-shaped velocity profile is due to the interaction between the shrinkage-induced flow and the positive solutal gradient adjacent to the liquidus interface. However, as the density inversion is caused by shrinkage effects, the corresponding buoyancy force is not strong enough to create an upward flow, even though the original parabolic velocity profile is distorted to a W-shaped.

Comparison of the solidified species concentration distribution calculated by the present study and the experimental results by Kato and Cahoon [6] is given in Fig. 6. It is noted that only the solidified portion of the alloy is plotted in the figure, and there is a moving

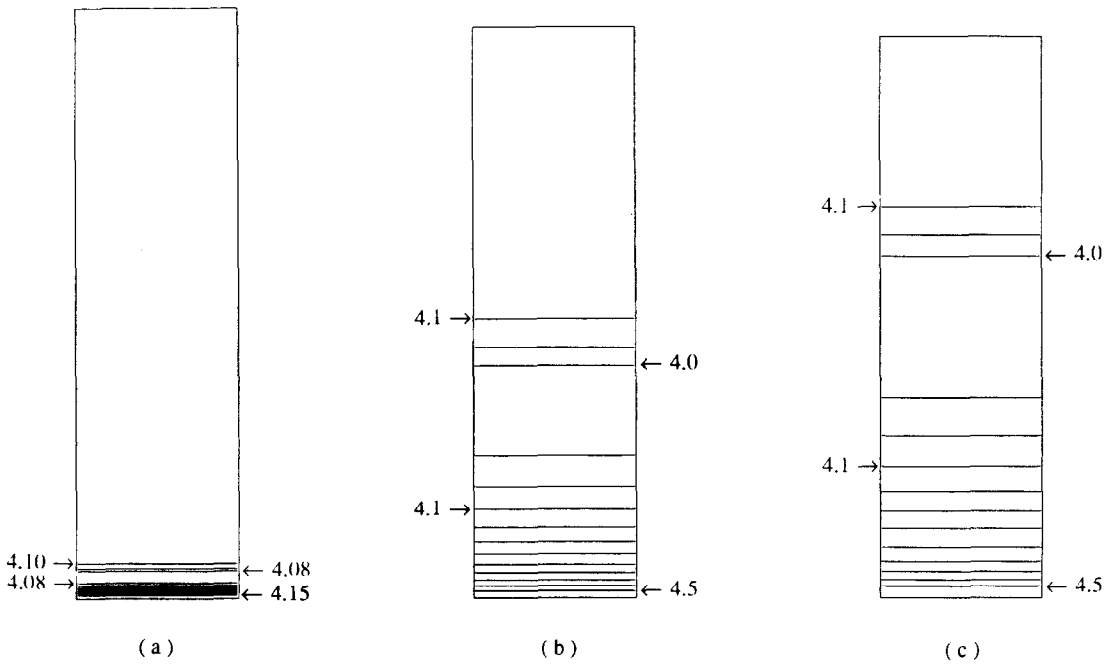

FIG. 4. The predicted isocomposition contours, in % copper, at times: (a) $t = 16.0$ s; (b) $t = 186.0$ s; (c) $t = 296.0$ s.

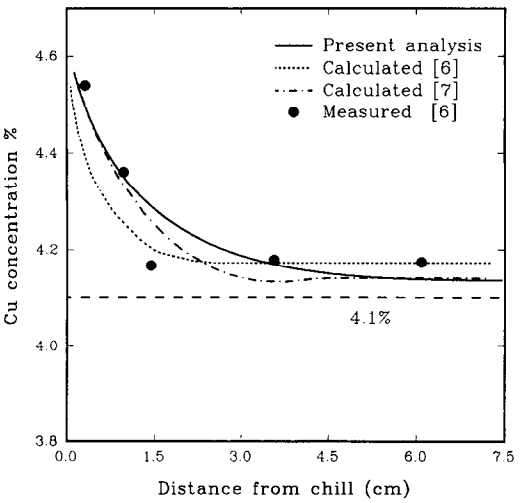

FIG. 6. Comparison of the final solidified solute distribution by this study and the measured and calculated ones by some previous studies.

negative-segregated mushy zone at a distance further away from the chill, which is not shown in the figure. As no information is available regarding the uncertainty analysis of the experimental measurements in the cited literature, it is felt that a direct comparison (i.e. % error) between the experimental data and the prediction by the present model is not appropriate. However, as seen in Fig. 6 the calculated results in this study are generally in good agreement with the experimental data. It is also noted that only the solute distribution in the solidified alloy is available from the literature, and the transient phenomena of the W-shaped velocity profile as well as the existence of negative-segregated mushy zone, discovered in the present study, were not reported before. The calculated results by Kato and Cahoon [6] and Ohnaka and Matsumoto [7] are also shown in the figure. Those results are obtained based on simpler models, which cannot be extended to multi-dimensional problems.

CONCLUSIONS

The inverse segregation for a unidirectional solidification of aluminum–copper alloys cooled from the bottom has been successfully predicted by the present mathematical model. It was found that the inverse segregation is caused by the fluid flow of solute-rich liquid in the mushy zone due to solidification contraction. The inverse segregation is accompanied by a negative-segregated mushy zone, which is moved and expanded away from the chill with time. A W-shaped velocity profile was created due to the interaction of shrinkage-induced flow and the buoyancy force caused by the positive solutal gradients in the mushy zone adjacent to the liquidus interface. The predicted copper concentration distribution in the solidified alloy is in good agreement with the published experimental data and the previously calculated results.

Acknowledgement—This study was supported in part by the Air Force Office of Scientific Research under Contract No. F49620-88-C-0053/SB5881-0378, which is gratefully acknowledged.

REFERENCES

1. M. C. Flemings and G. E. Nereo, Macrosegregation: Part I, *The Metallurgical Society of AIME* **239,** 1449–1461 (1967).
2. M. C. Flemings, *Solidification Processing*. McGraw-Hill, New York (1974).
3. E. Scheil, Beitrag zum problem der blockseigerung, *Metallforschung* **2,** 69–75 (1947).
4. J. S. Kirkaldy and W. V. Youdelis, Contribution to the theory of inverse segregation. *The Metallurgical Society of AIME* **212,** 833–840 (1958).
5. M. C. Flemings and G. E. Nereo, Macrosegregation: Part III, *The Metallurgical Society of AIME* **242,** 50–55 (1968).
6. H. Kato and J. R. Cahoon, Inverse segregation in directionally solidified Al–Cu–Ti alloys with equiaxed grains, *Metallurgical Trans.* **16A,** 579–587 (1985).
7. I. Ohnaka and M. Matsumoto, Computer simulation of macrosegregation in ingots, *Tetsu-to-Hagané (J. Iron Steel Inst. Jpn.)* **73,** 1698–1705 (1987).
8. I. Ohnaka and M. Matsumoto, Flow analysis during solidification by the direct finite difference method, *Trans. Iron Steel Inst. Jpn.* **26,** 781–789 (1986).
9. C. Beckermann and R. Viskanta, Double-diffusive convection during dendritic solidification of a binary mixture, *PCH PhysicoChemical Hydrodynamics* **10,** 195–213 (1988).
10. D. G. Neilson and F. P. Incropera, Unidirectional solidification of a binary alloy and the effects of induced fluid motion, *Int. J. Heat Mass Transfer* **34,** 1717–1732 (1991).
11. W. D. Bennon and F. P. Incropera, A continuum model for momentum, heat and species transport in binary solid–liquid phase change systems—I. model formulation, *Int. J. Heat Mass Transfer* **30,** 2161–2170 (1987).
12. K. C. Chiang and H. L. Tsai, Shrinkage-induced fluid flow and domain change in two-dimensional alloy solidification, *Int. J. Heat Mass Transfer* **35,** 1763–1770 (1992).
13. K. C. Chiang and H. L. Tsai, Interaction between shrinkage-induced fluid flow and natural convection during alloy solidification, *Int. J. Heat Mass Transfer* **35,** 1771–1778 (1992).
14. J. H. Chen, Shrinkage-induced fluid flow and its effect on the formation of macrosegregation during alloy solidification, Appendix A, Ph.D. Dissertation, University of Missouri-Rolla, Rolla, MO (1992).
15. P. C. Carman, Fluid flow through granular beds, *Trans. of the Institution of Chemical Engineers* **15,** 150–166 (1937).
16. K. Kubo and R. D. Pehlke, Mathematical modeling of porosity formation in solidification, *Metallurgical Trans.* **16A,** 823–829 (1985).
17. G. S. Beavers and E. M. Sparrow, Non-Dracy flow through fibrous porous media, *J. Appl. Mech.* **36,** 711–714 (1969).
18. R. D. Pehlke, A. Jeyarajan and H. Wada, *Summary of Thermal Properties for Casting Alloys and Mold Materials*, PB83-211003, National Information Service (1982).